Linear Circuit Models for On-Chip Quantum Electrodynamics

Alpár Mátyás,
Christian Jirauschek *Member, IEEE*, Federico Peretti, Paolo Lugli *Member, IEEE* and György Csaba

***Abstract*—We present equivalent circuits that model the interaction of microwave resonators and quantum systems. The circuit models are derived from a general interaction Hamiltonian. Quantitative agreement between the simulated resonator transmission frequency, qubit Lamb shift and experimental data will be shown. We demonstrate that simple circuit models, using only linear passive elements, can be very useful in understanding systems where a small quantum system is coupled to a classical microwave apparatus.**

***Index Terms*—cavity quantum electrodynamics, circuit modeling, coupled quantum-classical systems, quantum non demolition measurement**

I. Introduction

CAVITY quantum electrodynamics has long been an active field to study the interaction of electromagnetic radiation with matter, which is a fundamentally important topic in physics [1], [2], [3]. Recently, cavity quantum electrodynamic experiments were performed in the microwave regime [4], [5], [6], [7], where the cavity consisted of a high-quality factor (Q) microwave coplanar resonator. The quantum system was a charge qubit built from two Josephson junctions. Similar experiments were proposed to bring other nanosystems (molecules [8], nanomagnets [9], [10], flux qubits [10], [11], [12]) into interaction with coplanar waveguides. One of the most promising aspects of these experiments is that they can provide circuits which integrate quantum mechanical behavior and 'conventional' (high-frequency) components on a chip.

It is well established how to construct circuit models from electromagnetic models for commonly used active or passive components, which obey 'classical' circuit theory. It has been also demonstrated how one can build equivalent circuit models of basic two-state quantum systems [13]. The goal of the present paper is to show a systematic approach for building circuit models for an interacting resonator-quantum system, using linear approximations. This can be useful for developing quantum systems coupled via a resonator [14] or modeling the large external circuitry coupled to the quantum system. The possibility of this modeling approach was mentioned in [5]; to our knowledge, though, our paper is the first to analyze and exploit this model in detail. We investigate an experimental setup, similar to the one in [15], composed of a high-Q, superconducting microwave resonator, electrically coupled to a quantum circuit (often referred as transmon-qubit [16]).

During the past years the field of circuit quantum electrodynamics went through a considerable growth. Many quantum phenomena known from optical and three dimensional microwave systems were also observed in circuit quantum electrodynamics and simulated, including systems of entangled quantum circuits [17] and resonators coupled via flux qubits [18]. Such quantum electrodynamic systems need further optimization of both the quantum bit and the resonator, such as increasing qubit decay times and optimizing resonator losses [19].

The natural application area of circuit models is the understanding of the interaction between a relatively complex 'classical' circuitry and a relatively simple quantum circuit. These models do not show new physics, but rather facilitate the engineering of coupled microwave-quantum systems.

II. Device geometry

The setup of a typical circuit quantum electrodynamic experiment is shown in Fig. 1. A main component is a superconducting coplanar waveguide resonator, displayed in Fig. 1 (a) (longitudinal section) and (b) (cross section). A superconducting resonator can easily reach an unloaded quality factor in the range of $Q_{unloaded} \approx 10^6$ [4], [20]. The loaded quality factor of the resonators is designed by using finger-type capacitors in the central strip. These typically determine the lifetime of the resonator field (which should be high) and also the duration of the measurement of the nanosystem (which should be low in order to avoid energy relaxation and decoherence of the quantum system). The superconducting resonator is practically lossless and close to resonance, its port to port behavior can be modeled by the circuit elements in Fig. 1 (c), where the LC parameters are:

$$\begin{aligned} C_r &= (Z_0\omega_r)^{-1}, \\ L_r &= Z_0\omega_r^{-1}. \end{aligned} \tag{1}$$

Here, Z_0 is the resonator impedance and ω_r is the resonator frequency. The $50\,\Omega$ external environment is represented by the load resistors R_{load} in Fig. 1 (c) which, together with the finger-type capacitors $C_1 \approx C_2$ in the circuit model and the

Manuscript received March 5, 2010; accepted September 14, 2010.

The authors are with the Institute for Nanoelectronics, Technische Universität München, Arcisstr. 21, D-80333 München, Germany (e-mail: alparmat@mytum.de; jirauschek@tum.de; federico_peretti2002@yahoo.it; lugli@tum.de)

G. Csaba is with the University of Notre Dame, 46656 Notre Dame, USA (e-mail: gcsaba@nd.edu)

Financial support was partially from the Emmy Noether program (DFG, JI115/1-1), SFB 631 priority program of the DFG, the Erasmus programme of the European Union and the Pázmány Péter Catholic University (ITK) of Budapest.

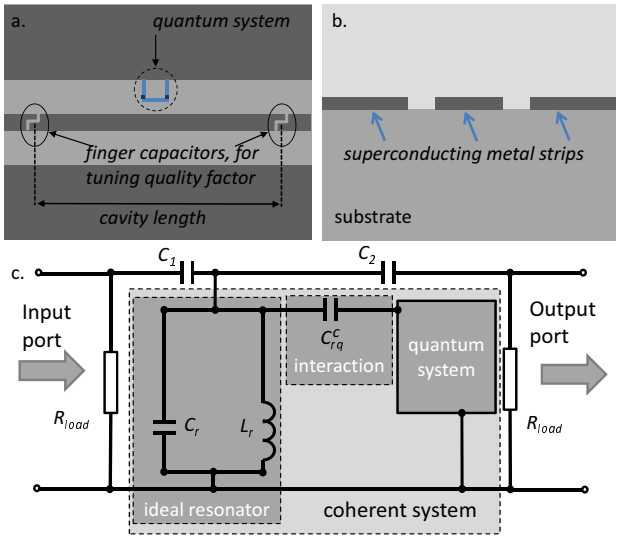

Fig. 1. Geometry-sketch of the (a) longitudinal section of the resonator, showing the quantum system-loop that is placed near the field maximum and (b) the cross section of the investigated coplanar waveguide resonator. The simplified equivalent circuit is shown in (c), representing the ideal resonator. Here, the capacitors C_1 and C_2 correspond to the finger capacitors at the two ends of the resonator, and the load resistors are also included. The coupling to the quantum system is capacitive.

resonator frequency ω_r, give the loaded quality factor of the resonator: $Q_{loaded} \approx 1/(R_{load}C_1\omega_r)$.

The quantum circuit is placed in the gap of the resonator (see Fig. 1 (a)) near the electric field maximum (magnetic field maximum) if it is an electrically (magnetically) interacting quantum system (i.e., charge qubit). Its presence slightly changes the values of the capacitance and inductance of the resonator and, thus, its resonance frequency.

The total system can be divided into a resonator part, an interaction part and a quantum system part. The coupling in the case of electrically interacting systems is capacitive.

Throughout this paper we will formulate our models assuming electrically coupled systems. We will also, however, mention the parameters for the magnetic case in the next section. Instead of modeling different geometries, the resonator will be considered as a lumped circuit. For more detailed investigation of resonator geometries, the reader is referred to [10], [12], [16].

III. Method

For the modeling of the interacting resonator-quantum system, we use a simplified (lossless) version of the circuit model in Fig. 1 (c), and the coupling to the environment is neglected. The Hamiltonian is obtained by adding the energy stored in the ideal (LC) resonator, the energy stored in the interaction of the resonator with the quantum system, and the energy of the quantum system:

$$H_{tot} = \overbrace{\frac{1}{2}\left(C_r\hat{V}_{res}^2 + L_r\hat{I}_{res}^2\right)}^{\text{ideal res. energy}} + \overbrace{\frac{\hbar g}{2V_{RMS}}\sigma_1\hat{V}_{res}}^{\text{interaction energy}} + \overbrace{\frac{\hbar\omega_q}{2}\sigma_3}^{\text{q. s. energy}} . \quad (2)$$

In the above equation, the different parts are illustrated by the boxes in Fig. 1 (c).

The resonator energy can be defined analogous to the classical energy of the LC circuit in Fig. 1 (c), however, the voltages and currents here are operators and their expectation value gives the voltage and current of the LC resonant circuit. The resonator root-mean square current (I_{RMS}) and voltage (V_{RMS}) [4], [5] is related to the minimum (or vacuum) field in the resonator. They are further discussed in Appendix A.

The interaction energy also contains the resonator voltage term ($\hat{V}_{res}$). Here, g is related to the geometric capacitance of the resonator-quantum system C^c_{rq}, and σ_1 is related to the voltage of the quantum system. The σ_i, in the QED framework, are referred to as Pauli matrices and are the basic observables of the two state quantum system. The interaction term is a standard term used in quantum electrodynamics, and valid for every electrically interacting quantum system and resonator.

The last term in (2), containing ω_q represents the energy level splitting ($\Delta E = \hbar\omega_q$) of the quantum system. This part can only be derived in terms of quantum mechanics.

For simulating the dynamics of the coupled system, we use the Liouville-von Neumann equation

$$\dot{A} = -\frac{j}{\hbar}\left[A, H_{tot}\right] \quad (3)$$

with the Hamiltonian of (2). Here A is an operator that represents either one of the Pauli matrices (σ_i) or the resonator voltage ($\hat{V}_{res}$) or current ($\hat{I}_{res}$) operator. Based on the von Neumann equation, we find the following coupled differential equation system:

$$\dot{\lambda}_1 = -\omega_q\lambda_2 - \frac{\lambda_1}{T_2} \quad (4)$$

$$\dot{\lambda}_2 = \omega_q\lambda_1 - g\lambda_3\frac{V_{res}}{V_{RMS}} - \frac{\lambda_2}{T_2} \quad (5)$$

$$\dot{\lambda}_3 = g\lambda_2\frac{V_{res}}{V_{RMS}} - \frac{\lambda_3 + 1}{T_1} \quad (6)$$

$$\frac{\dot{V}_{res}}{V_{RMS}} = \omega_r\frac{I_{res}}{I_{RMS}} - \gamma\frac{V_{res}}{V_{RMS}} \quad (7)$$

$$\frac{\dot{I}_{res}}{I_{RMS}} = -\omega_r\frac{V_{res}}{V_{RMS}} - g\lambda_1. \quad (8)$$

The above equations are a direct result of the von Neumann equation for the dissipationless case (if $T_1, T_2 \to \infty$ and $\gamma \to 0$). We can observe that the first three equations (4), (5) and (6) are the widely used Bloch equations [21] written for a two-level quantum system; the last two are equations for the dynamics of normalized resonator voltage and currents, thus we will call Eqs. (4)-(8) resonator-Bloch equations (RBEs). Dissipation is phenomenologically described by the decay and decoherence constants T_1 and T_2 [21], and the resonator loss,

$1/\gamma$ is added similar as in [22]. The λ_i variables are the expectation values of the Pauli matrices and represent the coherence vector characterizing the state of the quantum bit. The derivation of the resonator-Bloch equations is shown in Appendix A.

The only approximation used here is to neglect the correlations between the qubit and field [22], thus writing the expectation value of the normalized voltage and coherence vectors as a product of the individual expectation values:

$$\left\langle \sigma_i \hat{V}_{res} \right\rangle = \langle \sigma_i \rangle \left\langle \hat{V}_{res} \right\rangle = V_{res} \lambda_i. \tag{9}$$

An equation system similar to the resonator-Bloch equations was introduced by Jaynes and Cummings [22], [23], written for the coupling of electric fields and dipole moments. We now use this model to find passive circuits describing the interaction of the LC resonator-quantum system.

A. Modeling the system for large detuning

In circuit quantum electrodynamic experiments, measurements are often performed in the so-called dispersive regime, where the qubit-resonator detuning is much larger then the coupling frequency: $\Delta \gg g$. In this case, off-resonant interaction between the quantum system and the resonator does not switch the quantum system and λ_3 remains constant. Thus, we can neglect the oscillations of the inversion term in the resonator-Bloch equations ($\dot{\lambda}_3 = 0$) and perform a linear approximation by keeping $\lambda_3 = \lambda_3^0$. This is valid only if the measurement time is much smaller than the decay time T_1. For a large decay time T_1 or short measurement time window, the system behaves linearly, and the resonator-Bloch equations reduce to four coupled linear differential equations (we will call them linear resonator-Bloch equations): Eqs. (4), (5), (7) and (8) with $\lambda_3 = \lambda_3^0$. These can be modeled by the passive circuits shown in Fig. 2. These circuits represent the interaction of (a) electric and (b) magnetic quantum systems, with the resonator in the dispersive regime. Interaction between the quantum system and resonator occurs through their coupling capacitance in Fig. 2 (a) or mutual inductance in Fig. 2 (b), depending on the type of interaction (electric or magnetic).

In the circuit models, the decoherence time from resonator-Bloch equations (4) and (5) is represented by the parallel resistor with $R_q^1 C_q \approx T_2$; the series resistor, with $L_q/R_q^2 \approx T_2$ and the resonator decay rate γ, is given by $R_r C_r$ in case of electric and L_r/R_r in case of magnetic interactions. The parameters of the circuits were found as a direct result of the linear resonator-Bloch equations and are summarized in Table I; for the derivation see Appendix B. This table summarizes the central result of our work.

The physical parameters of the resonator are changed from the values in (1) to the values in Table I due to the presence of the quantum system. The circuit models presented in this section provide two resonance peaks in every case, which represent the oscillations of the coupled system. The coupling between the quantum system and the resonator changes the electromagnetic response of the resonator in a way that depends on the state (λ_3) of the quantum system. The quantum state can be read out non-destructively from the measurement on the resonator. In physics this is often referred to as quantum non-demolition measurement.

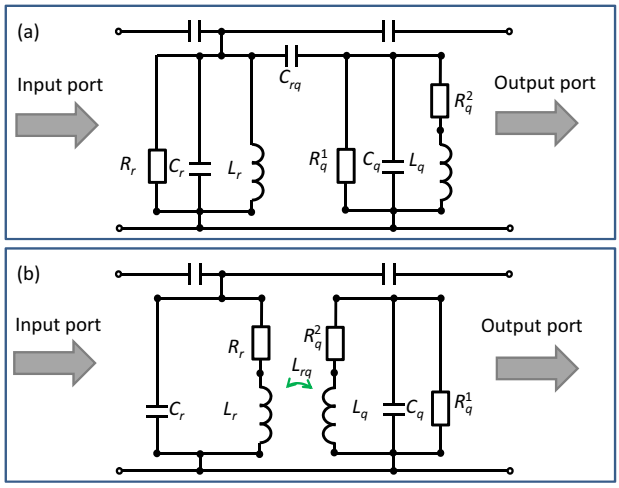

Fig. 2. Circuit models representing the linear quantum mechanical interaction of the resonator and the qubit (i.e., $\lambda_3 \approx \lambda_3^0$) in case of (a) electric interaction (e.g., charge qubit) and (b) magnetic interactions (e.g., flux qubit). The coupling between the resonator and quantum system in capacitive in (a) and inductive in (b). The quantum system behaves as a linear LC oscillator that changes the frequency of the resonator. The outcoupling capacitors, corresponding to the resonator finger-type gaps, have very small values and thus can be added to the resonant circuits that model the linear interaction.

B. Modeling the system in its ground state

Next, we will investigate the ground state of the coupled resonator-quantum system. We will also compare our simulation results mainly to measurements done in the ground state. In case of no applied field on the input port, the coupled resonator-quantum system will converge to the common ground state $[\lambda_1, \lambda_2, \lambda_3, V_{res}/V_{RMS}, I_{res}/I_{RMS}] = [0, 0, -1, 0, 0]$, due to the decay times T_1, T_2 and $1/\gamma$ in the resonator-Bloch equations. In the case of a small applied probe field on the resonator port, the system will oscillate around its ground state and the inversion remains unchanged (i.e., $\lambda_3 \approx -1$).

Rather than implementing the drive-fields in our resonator-Bloch equations, we start our simulations by taking a non-zero mode occupation of the resonator field. For this we take the initial condition: [0.04; 0; -0.999; 0; 0]. This corresponds to fields in the resonator-quantum system with an average photon number of approximately 0.01. Thus, for low fields in the resonator (approximately 0.01 photons [5], [15]), the nonlinear term $\lambda_2 V_{res}/V_{RMS}$ in the resonator-Bloch equations will oscillate near 0, as it is a product of two very small values. The inversion λ_3 will stay approximately constant and not change from its ground state even when the system has no detuning. As the inversion can be taken constant, the linear approximation done in the previous subsection holds, and we can take $\lambda_3^0 \approx -1$.

In the next section, we will compare our derived resonator-Bloch equation model and circuit models to experimental data, and show the validity of our approximations.

Interaction	R_q^1	R_q^2	L_q	C_q	R_r	L_r	C_r	C_{rq}/L_{rq}
Electric	$\omega_r T_2(-\lambda_3^0)Z_0$	$\frac{(-\lambda_3^0)Z_0\omega_r}{T_2\omega_q^2}$	$\frac{(-\lambda_3^0)Z_0\omega_r}{\omega_q^2}$	$\frac{1}{Z_0\omega_r(-\lambda_3^0)} - C_{rq}$	$Z_0\frac{\omega_q}{\gamma}$	$\frac{\omega_q Z_0}{\omega_r^2}$	$\frac{1}{Z_0\omega_q} - C_{rq}$	$\frac{g}{\omega_r\omega_q Z_0}$
Magnetic	$\frac{\omega_q^2 T_2 Z_0}{(-\lambda_3^0)\omega_r}$	$\frac{Z_0}{\omega_r T_2(-\lambda_3^0)}$	$\frac{Z_0}{\omega_r(-\lambda_3^0)} - L_{rq}$	$\frac{(-\lambda_3^0)\omega_r}{Z_0\omega_q^2}$	$Z_0\frac{\gamma}{\omega_q}$	$\frac{Z_0}{\omega_q} - L_{rq}$	$\frac{\omega_q}{Z_0\omega_r^2}$	$\frac{gZ_0}{\omega_r\omega_q}$

TABLE I
SUMMARY OF THE PARAMETERS CALCULATED FROM THE LINEAR RESONATOR-BLOCH EQUATIONS, IF THE INVERSION IS CONSTANT ($\lambda_3 \approx \lambda_3^0$).

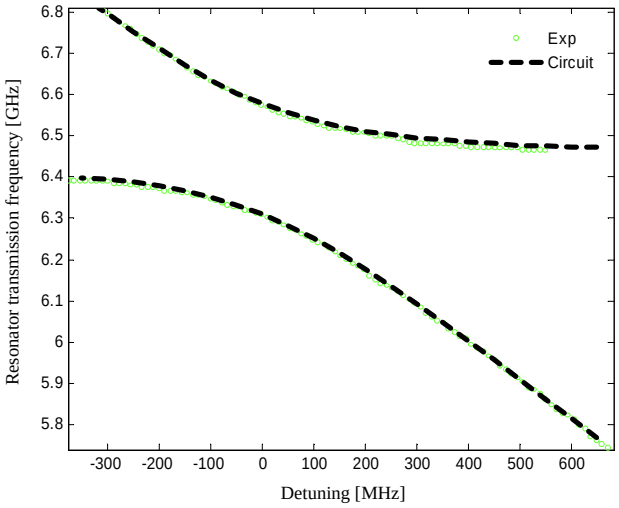

Fig. 3. Transmission frequency of the resonator as a function of detuning. Small circles represent experimental data from [15] and the dashed lines represent our circuit model. The anticrossing behavior is clearly visible and the separation is approximately given by the vacuum Rabi frequency at $\Delta = 0$. The excellent agreement confirms the usability of our circuit model to calculate cavity transmission.

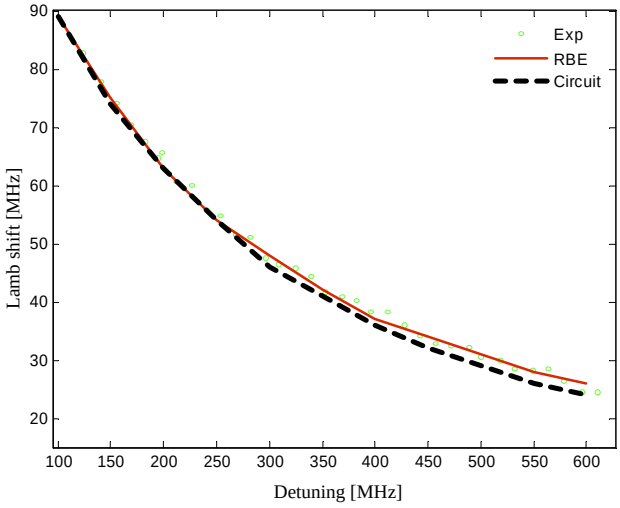

Fig. 4. Frequency (Lamb) shift of the quantum bit as a function of qubit detuning. Small circles represent experimental data. Continuous lines represent results extracted from the numerical solutions of the resonator-Bloch equations. Dashed lines indicate results of our passive circuit model (Fig. 2 (a))

IV. RESULTS

We performed numerical and circuit simulations on a recently measured resonator-transmon qubit device from [15]. We took as input parameters: resonator frequency $\omega_r/(2\pi) = 6.44$ GHz, impedance $Z_0 = 50\ \Omega$, vacuum Rabi frequency $g/(2\pi) = 266$ MHz and cavity decay rate $\gamma/(2\pi) = 1.6$ MHz. The dephasing time was approximately $T_2 \approx 1\ \mu$s, which is known to be in good agreement with experimental findings [16]. Further, the linewidth of the qubit coherence vector elements λ_1, λ_2 is in good agreement with the experiment (approximately 3 MHz) in [15]. Simulations were performed in LTSPICE [24] based on the presented circuit models, using frequency domain AC analysis.

The transmission of the circuit in Fig. 2 (a) was calculated for the above parameters, setting $\lambda_3^0 = -1$ as the system was in ground state. We investigated the dependence of the result with respect to quantum system frequency, while keeping the resonator frequency fixed. This was done by varying ω_q which was directly related to the parameters of our circuit model.

The empty circles in Fig. 3 represent data from [15] that has been transformed from flux to detuning coordinates so that our simulated results can be compared to the measured cavity transmission. We can see excellent agreement of the transmission frequency of our circuit (dashed line) with experimental data (small circles), for positive and negative detuning, showing the validity of the linear approximation and the excellent description of the anticrossing of the resonator-quantum system by the derived circuit model. At approximately $\Delta = 0$, the peaks are separated by the vacuum Rabi frequency $g/(2\pi)$. The transmission graphs do not contain amplitude data, but we mention here, that the reduction of the peak far from the resonator frequency ($\omega_r/(2\pi)$=6.44 GHz) is also observed in our simulation. In the case of large detuning, the peaks are highly separated and the qubit peak gets highly reduced, while the resonator frequency peak approaches the original resonator frequency; this shows that for large detuning the two systems are decoupled.

After successfully applying our circuit model to the description of the cavity transmission, we performed an analysis on the quantum bit frequency shift (Lamb shift). The cavity transmission was calculated as a function of the detuning; the Lamb shift was extracted by subtracting the bare cavity frequency and the detuning (Δ) from the simulated qubit frequency. This was done by solving the full resonator-Bloch equations (4)-(8) numerically using a basic Runge-Kutta solver and by employing our circuit models. The simulation results were compared to experimental data from [15], for a detuning ranging from 100 MHz to 600 MHz. The comparison was done by changing the frequency of the qubit and keeping the

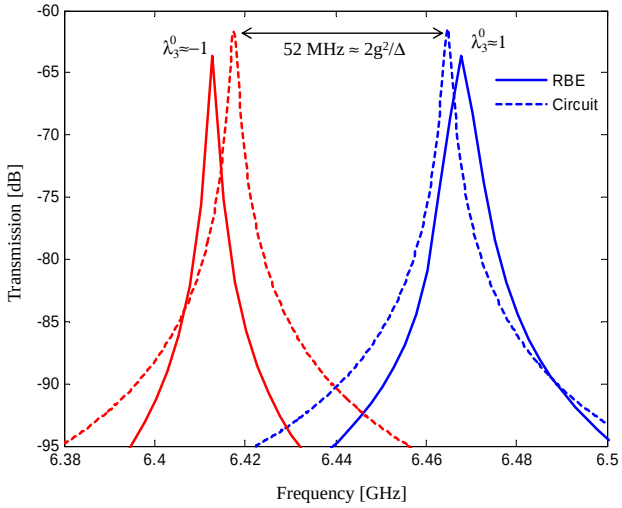

Fig. 5. Theoretical demonstration of our circuit model showing the state dependent resonator frequency shift, that opens the possibility of a quantum state measurement. The quantum system decay time was $20\,\mu s$, that was large enough not to influence the linewidth of the excited state. The shift is approximately g^2/Δ. The slight disagreement of the peak positions results from the Fourier transform on the finite simulation window of the output voltage signal calculated with the resonator-Bloch equations.

resonator frequency constant.

As shown in Fig. 4, we see an excellent agreement between the experimental Lamb shift (small empty circles) and the numerical solutions of the resonator-Bloch equations (solid line) as well as our linear circuit model (dashed line). Thus, we can affirm that also the frequency shift of the quantum system (Lamb shift) is well described by our circuit model. To this point we only did simulations of the quantum system in its ground state. For the numerical solution of the full resonator-Bloch equations, we used the initial conditions $[\lambda_1, \lambda_2, \lambda_3, V_{res}/V_{RMS}, I_{res}/I_{RMS}] = [0.04, 0, -0.999, 0, 0]$ as discussed in Section III-B. For the circuit model, we set $\lambda_3^0 = -1$.

We will now investigate the case, when the quantum system is away from its ground state, and its frequency is far detuned from the resonator frequency. In this case one can perform a non-demolition readout of the quantum state, i.e., read out the inversion without changing it. This can be done because, if the detuning tends to infinity (practically is large enough so that the inversion changes only slightly), then it is known from Rabi's solutions that the inversion will not change (i.e., the resonator is unable to switch the quantum circuit during measurement). For an optimal quantum state readout, however, the state of the quantum system should not decay during measurement. Based on our circuit model and resonator-Bloch equations presented earlier, we now estimate the value of the decay time T_1 for an optimal readout.

The quantum state readout measurement is performed in the dispersive regime, as discussed in Section III-A. In the case of small decay times T_1, if the quantum system is in its excited state, it will quickly relax to the ground state; this limits the measurement time and, thus, the Fourier window of our numerical simulations. On the other hand, for large decay times, the quantum-state dependent cavity shift can be simulated, as shown in Fig. 5. The simulated cavity-pull linewidths extracted from the Fourier transform of the numerical resonator-Bloch equation solutions and from the frequency domain simulation of our circuit model agree well. This shows that the broadening of the peaks is mainly due to decoherence T_2 and cavity decay $(1/\gamma)$ and not the qubit decay T_1, which was not included in the circuit model. In this limit, the quantum-state dependent cavity pull is resolvable, and we find that for this case $T_1 \geq 20\ \mu s$ (or more) would be required, so that the two linewidths approximately agree. For smaller decay times, the numerical simulations of the resonator-Bloch equations show high asymmetry of the two peaks due to the non-Lorentzian behavior of the spectral line corresponding to the excited qubit state ($\lambda_3^0 = 1$); this is due to the decay of the state during simulation. In order to avoid the decay of the quantum state the simulation window can be reduced. For a too small simulation window, however, the Fourier transform of the signal becomes inaccurate.

V. Conclusions

We have derived circuit models for the understanding and modeling of superconducting coplanar waveguide resonators interacting with quantum systems. They can easily be used to model the cavity transmission, Lamb shift and quantum non-demolition measurement. We find their application straightforward in understanding experimental data and estimating decay times for an optimal quantum state readout. Our models can be extended, e.g., by adding further circuits to represent additional qubits. Also, embedding quantum systems in large-scale classical circuitry is straightforward in our circuit models.

Acknowledgment

The authors are grateful to Prof. Árpád Csurgay and Prof. Wolfgang Porod for initiating their research on circuit models of quantum systems. The work on resonators started in collaboration with Prof. Rudolph Gross.

Appendix A
Derivation of the Resonator-Bloch Equations

For the derivation of the resonator-Bloch equations, we need to review a few concepts widely used and well established in quantum optics. The starting point is to define the resonator voltage, similar as in [4], [5]. The voltages and currents on the LC circuit are defined as:

$$V_{RMS}^{-1}\hat{V}_{res} = a + a^+, \tag{10}$$

$$I_{RMS}^{-1}\hat{I}_{res} = -j(a - a^+). \tag{11}$$

Here the terms a^+ and a represent the emission and absorption operators. The commutator properties of these operators are

$$[a, a^+] = 1, [a, a^+a] = a, [a^+, a^+a] = -a^+,$$
$$[a, a] = [a^+, a^+] = [a^+a, a^+a] = 0. \tag{12}$$

The brackets represent a commutator relation (also used in the von Neumann equation (3)).

The normalization terms V_{RMS} and I_{RMS} represent the root-mean square voltage and current [4], [5], on the resonator:

$$V_{RMS} = \sqrt{\hbar\omega_r/(2C_r)}, \tag{13}$$
$$I_{RMS} = \sqrt{\hbar\omega_r/(2L_r)}. \tag{14}$$

If we substitute the voltage and current operators ((10) and (11)) into the general Hamiltonian shown in (2) and use the commutator operations defined in (12), we can get the general Hamiltonian

$$H_{tot} = \overbrace{\hbar\omega_r a^+ a}^{\text{ideal res. energy}} + \overbrace{\frac{\hbar g}{2}\sigma_1(a+a^+)}^{\text{interaction energy}} + \overbrace{\frac{\hbar\omega_q}{2}\sigma_3}^{\text{q. s. energy}}, \tag{15}$$

widely used in cavity quantum electrodynamics [5], [21], [25], [26].

For each Pauli matrix $\sigma_i, (i = 1, 2, 3)$ and for the normalized current and voltage in (10) and (11), we used the von Neumann equation (3) for finding the resonator-Bloch equations.

We now show the derivation of the dynamic equation for the resonator normalized current (8). The other resonator-Bloch equations (for coherence vector and resonator normalized voltage) can be derived analogously. First, the normalized current can be written as

$$I_{RMS}^{-1}\partial_t \hat{I}_{res} = -j\hbar^{-1}\left[I_{RMS}^{-1}\hat{I}_{res}, H_{tot}\right] = -j\hbar^{-1}I_{RMS}^{-1}\left(\hat{I}_{res}H_{tot} - H_{tot}\hat{I}_{res}\right). \tag{16}$$

Using the properties of the creation/annihilation operators from (12), the above von Neumann equation simplifies to

$$I_{RMS}^{-1}\partial_t \hat{I}_{res} = -\omega_r(a+a^+) - g\sigma_1. \tag{17}$$

Using the definition in (10) and taking the expectation values of the time dependent variables in the above equation, we get (8).

APPENDIX B
DERIVATION OF THE EQUIVALENT LINEAR CIRCUIT

If the inversion is constant ($\lambda_3 = \lambda_3^0$) and the system does not decay (i.e., $T_1 \to \infty$), we can linearize the resonator-Bloch equations and thus get an equivalent circuit. In this case (6) is automatically fulfilled, and the other resonator-Bloch equations (4), (5), (7) and (8) simplify to the linear differential equation system:

$$\dot{\lambda}_1 = -\omega_q\lambda_2 - T_2^{-1}\lambda_1 \tag{18}$$
$$\dot{\lambda}_2 = \omega_q\lambda_1 - g\lambda_3^0 V_{RMS}^{-1}V_{res} - T_2^{-1}\lambda_2 \tag{19}$$
$$V_{RMS}^{-1}\dot{V}_{res} = I_{RMS}^{-1}\omega_r I_{res} - \gamma V_{RMS}^{-1}V_{res} \tag{20}$$
$$I_{RMS}^{-1}\dot{I}_{res} = -V_{RMS}^{-1}\omega_r V_{res} - g\lambda_1. \tag{21}$$

By rewriting the above as two second order equations, we get:

$$\ddot{\lambda}_2 = -\omega_q^2\lambda_2 - T_2^{-1}\omega_q\lambda_1 - g\lambda_3^0 V_{RMS}^{-1}\dot{V}_{res} - T_2^{-1}\dot{\lambda}_2 \tag{22}$$
$$I_{RMS}^{-1}\ddot{I}_{res} = V_{RMS}^{-1}\omega_r\gamma V_{res} - I_{RMS}^{-1}\omega_r^2 I_{res} - g\dot{\lambda}_1. \tag{23}$$

The above equations can be equivalently found by using:

$$\dot{\lambda}_1 = -\omega_q\lambda_2 - \omega_q^{-1}V_{RMS}^{-1}g\lambda_3^0\dot{V}_{res} - T_2^{-1}\lambda_1 \tag{24}$$
$$\dot{\lambda}_2 = \omega_q\lambda_1 - T_2^{-1}\lambda_2 \tag{25}$$
$$\dot{V}_{res} = \omega_r Z_0 I_{res} + \omega_r^{-1}gV_{RMS}\dot{\lambda}_1 - \gamma V_{res} \tag{26}$$
$$\dot{I}_{res} = -Z_0^{-1}\omega_r V_{res}. \tag{27}$$

Introducing the quantum system voltage and current as:

$$V_q = V_{RMS}\lambda_1, \tag{28}$$
$$I_q = (-\lambda_3^0)^{-1}\omega_r^{-1}I_{RMS}\omega_q\lambda_2, \tag{29}$$

(24)-(27) change into equations for two capacitively coupled resonant circuits, with parameters shown in Table I.

REFERENCES

[1] H. Mabuchi and A. C. Doherty, "Cavity Quantum Electrodynamics: Coherence in Context," *Science*, vol. 298, pp. 1372–1377, Nov. 2002.

[2] P. R. Berman(ed), *Cavity Quantum Electrodynamics*. Academic Press, Boston, 1994.

[3] H. Carmichael, *An Open Systems Approach to Quantum OpticsCavity Quantum Electrodynamics*. Springer, Berlin, 1993

[4] A. Wallraff, D. I. Schuster, A. Blais, L. Frunzio, R.-S. Huang, J. Majer, S. Kumar, S. M. Girvin, and R. J. Schoelkopf, "Strong coupling of a single photon to a superconducting qubit using circuit quantum electrodynamics," *Nature*, vol. 431, pp. 162–167, Sep. 2004.

[5] A. Blais, R.-S. Huang, A. Wallraff, S. M. Girvin, and R. J. Schoelkopf, "Cavity quantum electrodynamics for superconducting electrical circuits: An architecture for quantum computation," *Phy. Rev. A*, vol. 69, no. 6, pp. 062320-1–062320-11, Jun. 2004.

[6] D. I. Schuster, A. A. Houck, J. A. Schreier, A. Wallraff, J. M. Gambetta, A. Blais, L. Frunzio, J. Majer, B. Johnson, M. H. Devoret, S. M. Girvin, and R. J. Schoelkopf, "Resolving photon number states in a superconducting circuit," *Nature*, vol. 445, pp. 515–518, Feb. 2007.

[7] F. Deppe, M. Mariantoni, E. P. Menzel, A. Marx, S. Saito, K. Kakuyanagi, H. Tanaka, T. Meno, K. Semba, H. Takayanagi, E. Solano, and R. Gross, "Two-photon probe of the Jaynes Cummings model and controlled symmetry breaking in circuit QED," *Nat. Phys.*, vol. 4, pp. 686–691, Sep. 2008.

[8] A. André, D. Demille, J. M. Doyle, M. D. Lukin, S. E. Maxwell, P. Rabl, R. J. Schoelkopf, and P. Zoller, "A coherent all-electrical interface between polar molecules and mesoscopic superconducting resonators," *Nat. Phys.*, vol. 2, pp. 636–642, Sep. 2006.

[9] J. Tejada, E. M. Chudnovsky, E. del Barco, J. M. Hernandez, and T. P. Spiller, "Magnetic qubits as hardware for quantum computers," *Nanotechnology*, vol. 12, pp. 181–186, Jun. 2001.

[10] G. Csaba, A. Matyas, F. Peretti, and P. Lugli, "Circuit modeling of coupling between nanosystems and microwave coplanar waveguides," *Int. J. Circ. Theor. Appl.* , vol. 35, no. 3, pp. 315–324, Apr. 2007.

[11] T. Lindström, C. H. Webster, J. E. Healey, M. S. Colclough, C. M. Muirhead, and A. Y. Tzalenchuk, "Circuit QED with a flux qubit strongly coupled to a coplanar transmission line resonator," *Supercond. Sci. Tech.*, vol. 20, pp. 814–821, Aug. 2007.

[12] G. Csaba, Z. Fahem, F. Peretti, and P. Lugli, "Circuit modeling of flux qubits interacting with superconducting waveguides," *J. Comp. Elect.*, vol. 6, pp. 105–108, Jan. 2007.

[13] A. I. Csurgay and W. Porod, "Equivalent circuit representation of arrays composed of coulomb-coupled nano-scale devices: modeling, simulation and realizability," *Int. J. Circ. Theor. Appl.*, vol. 29, no. 1, pp.3–35, Jan. 2001.

[14] J. Majer, J. M. Chow, J. M. Gambetta, J. Koch, B. R. Johnson, J. A. Schreier, L. Frunzio, D. I. Schuster, A. A. Houck, A. Wallraff, A. Blais, M. H. Devoret, S. M. Girvin, and R. J. Schoelkopf, "Coupling superconducting qubits via a cavity bus," *Nature*, vol. 449, pp. 443–447, Sep. 2007.

[15] A. Fragner, M. Göppl, J. M. Fink, M. Baur, R. Bianchetti, P. J. Leek, A. Blais, and A. Wallraff, "Resolving Vacuum Fluctuations in an Electrical Circuit by Measuring the Lamb Shift," *Science*, vol. 322, pp. 1357–1360, Nov. 2008.

[16] A. A. Houck, J. A. Schreier, B. R. Johnson, J. M. Chow, J. Koch, J. M. Gambetta, D. I. Schuster, L. Frunzio, M. H. Devoret, S. M. Girvin, and R. J. Schoelkopf, "Controlling the Spontaneous Emission of a Superconducting Transmon Qubit," *Phys. Rev. Lett.*, vol. 101, no. 8, pp. 080502-1–080502-4, Aug. 2008.

[17] A. Blais, J. Gambetta, A. Wallraff, D. I. Schuster, S. M. Girvin, M. H. Devoret, and R. J. Schoelkopf, "Quantum-information processing with circuit quantum electrodynamics," *Phys. Rev. A*, vol. 75, no. 3, pp. 032329-1–032329-21, Mar. 2007.

[18] G. M. Reuther, D. Zueco, F. Deppe, E. Hoffmann, E. P. Menzel, T. Weißl, M. Mariantoni, S. Kohler, A. Marx, E. Solano, R. Gross, and P. Hänggi, "Two-resonator circuit quantum electrodynamics: Dissipative theory," *Phys. Rev. B*, vol. 81, no. 14, p. 144510-1–144510-16, Apr 2010.

[19] D. Williams and S. Schwarz, "Design and performance of coplanar waveguide bandpass filters," *Trans. Microw. Theory Tech.*, vol. 31, no. 7, pp. 558–566, jul. 1983.

[20] L. Frunzio, A. Wallraff, D. Schuster, J. Majer, and R. Schoelkopf, "Fabrication and characterization of superconducting circuit QED devices for quantum computation," *Trans. Appl. Supercond.*, vol. 15, no. 2, pp.860–863 Nov. 2004.

[21] L. Allen and J. H. Eberly, *Optical Resonance and Two Level Atoms*. Wiley, New York, 1975.

[22] E. T. Jaynes and F. W. Cummings, "Comparison of Quantum and Semiclassical Radiation Theories with Application to the Beam Maser," *P IEEE*, vol. 51, no. 1 pp.89–109, Sep. 1962.

[23] F. W. Cummings, "Comparison of Quantum and Semiclassical Radiation Theories with Application to the Beam Maser." Ph.D. dissertation, STANFORD UNIVERSITY, 1962.

[24] *Linear Technology*. [Online]. Available: http://www.linear.com/designtools/software/

[25] J. Shen and S. Fan, "Coherent Single Photon Transport in a One-Dimensional Waveguide Coupled with Superconducting Quantum Bits," *Phys. Rev.Lett.*, vol. 95, no. 21, pp. 213001-1–213001-4, Nov. 2005.

[26] D. F. Walls and G. J. Milburn, *Quantum optics*. Springer, Berlin, 1995.

Alpár Mátyás Alpár Mátyás was born in Aiud, Romania, in 1983. He received his M.Sc. degrees in electrical engineering from the Pázmány Péter Catholic university of Budapest, in 2007.

Since 2007 he is a Ph.D. student at the TU München in Germany. His main research interests are modeling and optimizing quantum cascade lasers in the THz and infrared regimes and simulations including the interaction between resonators and quantum systems.

Christian Jirauschek Christian Jirauschek was born in Karlsruhe, Germany, in 1974. He received his Dipl-Ing. and doctoral degrees in electrical engineering in 2000 and 2004, respectively, from the Universität Karlsruhe (TH), Germany.

From 2002 to 2005, he was a Visiting Scientist at the Massachusetts Institute of Technology (MIT), Cambridge, MA. Since 2005, he has been with the TU München in Germany, first as a Postdoctoral Fellow and since 2007 as the Head of an Independent Junior Research Group (Emmy-Noether Program of the DFG). His research interests include modeling in the areas of optics and device physics, especially the simulation of quantum devices and mode-locked laser theory.

Dr. Jirauschek is a member of the IEEE, the German Physical Society (DPG), and the Optical Society of America. Between 1997 and 2000, he held a scholarship from the German National Merit Foundation (Studienstiftung des Deutschen Volkes).

Federico Peretti Federico Peretti was born in Fermo, Italy in 1980. He received his degree in electronic engineering and doctoral degree in electromagnetism and bioengineering in 2005 and 2009, respectively, from the Università Politecnica Delle Marche, Italy. From 2006 to 2009 he was Scientist at the Institute for Nanoelectronics at the Technische Universität München, where his interests included modeling in the areas of microwaves and of quantum devices, especially the simulation of coplanar resonators for interactions with two-level systems.

Paolo Lugli Paolo Lugli graduated in Physics at the University of Modena, Italy, in 1979. In 1981 he joined Colorado State University, Fort Collins, CO, where he received his Master of Science in 1982 and his Ph.D. in 1985, both in Electrical Engineering. In 1985 he joined the Physics Department of the University of Modena as Research Associate. From 1988 to 1993 he was Associate Professor of "Solid State Physics" at the "Engineering Faculty" of the 2nd University of Rome "Tor Vergata". In 1993 he was appointed as Full Professor of "Optoelectronics" at the same university. In 2003 he joined the Technische Universität München where he was appointed head of the newly created Institute for Nanoelectronics.He is author of more than 250 scientific papers and co-author of the books "The Monte Carlo Modelling for Semiconductor Device Simulations" (Springer, 1989) and "High Speed Optical Communications" (Kluver Academic, 1999). In 2004, he served as General Chairman of the IEEE International Conference on Nanotechnology held in Munich.

His current research interests involve the modeling, fabrication and characterization of organic devices for electronics and optoelectronics applications, the design of organic circuits, the numerical simulation of microwave semiconductor devices, and the theoretical study of transport processes in nanostructures.

György Csaba György Csaba was born in Budapest, Hungary, in 1974. He received the M.Sc. degree from the Technical University of Budapest in 1998 and his PhD degree from the University of Notre Dame in 2003. From 2004 to 2009 he worked as a Research Assistant at the Technische Universität München, Germany and in 2010 he joined the faculty of the university of Notre Dame as a research assistant professor. His research interests are in circuit-level modeling of nanoscale systems (especially magnetic devices) and exploring their applications for nonconventional architectures, such as magnetic computing and physical cryptography.